Intermetallics 136 (2021) 107239

Contents lists available at ScienceDirect

Intermetallics

journal homepage: www.elsevier.com/locate/intermet

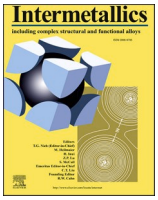

Effect of Fe on the Hall-Petch relationship of $(CoCrMnNi)_{100-x}$ Fe_x medium-and high-entropy alloys

Ibrahim Ondicho [a,c,*], Bernard Alunda [b], Nokeun Park [c,**]

[a] Department of Mechanical Engineering, Dedan Kimathi University of Technology, P.O Box 657-10100, Nyeri, Kenya
[b] School of Mining and Mineral Processing, Taita Taveta University, P.O Box 2176-20030, Voi, Kenya
[c] School of Materials Science and Engineering, Yeungnam University, Gyeongsan, 38541, Republic of Korea

ARTICLE INFO

Keywords:
A. high-entropy alloys
B. Yield stress
C. Heat treatment
D. Grain boundary
F. mechanical testing

ABSTRACT

In the present study, a systematic investigation on the effect of Fe content on the Hall-Petch coefficient of $(CoCrMnNi)_{100-x}$ Fe_x (x = 20, 40, 50, and 60) medium- and high-entropy alloys (M/HEAs) was carried out. The cold-rolled alloys were annealed at 900 °C and 1000 °C between 3 min and 10 h for recrystallization. Scanning electron microscope with a backscattered detector was used to obtain micrographs of recrystallized specimens for grain size calculation. Tensile testing was used to evaluate the mechanical properties of the alloys. The microstructure showed that regardless of the alloy composition, the grain size was approximately similar when subjected to the same heat treatment condition. Moreover, all the alloys obeyed the classical Hall-Petch relationship. Friction stress (solid solution, SS strengthening) decreased with an increase of Fe content, which was attributed to weak lattice distortion caused by the reduction of the atomic size misfit. The Hall-Petch coefficient, which represents grain boundary (GB) strengthening, also decreases as the Fe content increases. A linear relationship between intrinsic stacking fault energy and Hall-Petch coefficient was found not to exist. However, it is proposed that the monotonic decrease of the Hall-Petch coefficient is directly related to the unstable stacking fault energy (γ_{USFE}). As a result, an increase of Fe content in $(CoCrMnNi)_{100-x}$ Fe_x alloy system leads to an increase of γ_{USFE}, which in turn weakens GB strengthening (Hall-Petch coefficient). Moreover, HEAs and MEAs with higher Fe content tend to have low yield strength due to weak contributions from both SS and GB strengthening. Therefore, to design superior MEAs and HEAs with enhanced strength, the choice of principal elements and their respective contents is imperative for an optimized contribution from both SS and GB strengthening mechanisms.

1. Introduction

High entropy alloys (HEAs) have received tremendous scientific attention as they tend to possess superior physical and mechanical properties compared to the conventional alloys. This paradigm shift is attributed to the quest for scientists and engineers to develop alloys that can operate in practically demanding environments. Therefore, harnessing the proposed high strength of HEAs becomes an interesting adventure. HEAs are often defined as alloys with five or more principal elements with a concentration range of 5–35 at.% while that of medium-entropy alloys (MEAs) as alloys having four or less principal elements in equiatomic or near equiatomic [1,2]. Initially, research was confined to finding single-phase alloys with simple solid solution crystal structures such as face-centered cubic (fcc), body-centered cubic (bcc), and hexagonal close-packed (hcp) [3,4]. Of the three crystal structures, fcc HEAs have been widely studied because their compositions and microstructures are easily tunable to obtain high ductility [5]. However, their impressive ductility is mostly preceded by low yield and tensile strengths (YS/UTS). Therefore, several attempts have been made to improve the strength of fcc HEAs, which include precipitation hardening (PP), solid solution strengthening (SS), transformation- and twinning induced plasticity (TRIP/TWIP), and grain boundary (GB) strengthening [6-13]. The first four mechanisms (PP, SS, TRIP, and TWIP), have been widely used in improving mechanical properties of HEAs compared to GB. This is so against the backdrop of alloy design complexities and possibly cost, when some of these strengthening mechanisms are invoked. For instance, to trigger TRIP/TWIP in some HEAs, the alloy composition has to be engineered in such a way that the stacking fault

* Corresponding author. Department of Mechanical Engineering, Dedan Kimathi University of Technology, P.O Box 657-10100, Nyeri, Kenya.
** Corresponding author.
E-mail addresses: ibrahim.ondicho@dkut.ac.ke (I. Ondicho), nokeun_park@yu.ac.kr (N. Park).

https://doi.org/10.1016/j.intermet.2021.107239
Received 10 February 2021; Received in revised form 15 May 2021; Accepted 16 May 2021

energy (SFE) is significantly reduced [9,14,15]. This ingenious variation of the chemical composition of HEAs can, sometimes, lead to costly alloys especially when elements such as Co are used to obtain reduced SFE values [16].

On other hand, GB strengthening is an inherent mechanism of any particular alloy and can be easily harnessed by suitable thermo-mechanical processing without a complicated approach in alloy design. This type of strengthening is well expressed by the classical Hall-Petch relationship (HP), which relates the grain size with theYS.

$$\sigma_y = \sigma_o + K_y d^{-\frac{1}{2}} \quad (1)$$

where σ_y is the YS, σ_o is the friction stress, K_y is the HP coefficient, and d is the mean grain size. Liu et al. [17] measured hardness as a function of grain size in the equiatomic CoCrFeMnNi HEA and found that the alloy follows the HP relationship but with a higher hardening coefficient compared to the conventional alloys. Moreover, for the similar alloy, Otto et al. [13] reported a HP coefficient of 494 MPa $\times$ $\mu m^{-1/2}$ using tensile test data carried out at room temperature. In addition, they demonstrated that temperature has an effect on the HP coefficient, in that it is higher at 77 K (538 MPa $\times$ $\mu m^{-1/2}$) and then decreases as testing temperature is raised to 1073 K (127 MPa $\times$ $\mu m^{-1/2}$). Other studies have been carried out both at room temperature [18-20] and low or high temperatures [13,21]. However, apart from the effect of temperature on the HP relationship [13,21], there is limited literature about other factors affecting GB strengthening (HP coefficient) at room temperature considering that there is a variation as the composition of an alloy changes. In the present study, we carried out an investigation on the effect of changing Fe content on the mechanical properties of an equiatomic CoCrFeMnNi HEA. Interestingly, both the friction stress and HP coefficient decrease as the Fe content increase $(CoCrMnNi)_{100-x}$ Fe_x, which means that SS and GB strengthening mechanisms are inferior in the non-equatomic HEAs with higher Fe. Finally, the possible factors for such phenomenon are postulated and discussed.

2. Experimental methods

2.1. Ingot preparation

The $(CoCrMnNi)_{100-x}$ Fe_x HEAs and MEAs (where x = 20, 40, 50, and 60 at.%) were produced by arc-melting technique in a water-cooled copper mould with the raw materials having a purity > 99.98 at.%. Prior to melting, the pure elements were cleaned using SiC paper to remove any possible oxide layer. To compensate for the easy evaporation of Mn, 1% was added. The alloys were flipped and re-melted for at least five times to minimize chemical inhomogeneity.

2.2. Heat treatment

The as-cast materials were homogenized at 1000 °C for 24 h under argon gas to remove any remaining chemical micro-segregation before water-quenching. The cylindrical cast ingots with a dimensions Ø15 $\times$ 120 mm were cold rolled with a 90% thickness reduction (final thickness ~1.5 mm). Heat treatment specimens were obtained from the mid-section of the rolling-normal plane (RD-ND) of the cold-rolled plate and annealed at 900 °C for 3 min, 15 min, 1 h and 2 h, and at 1000 °C for 2 h and 10 h to obtain microstructures of various grain sizes (fine to coarse). The annealed specimens were water-quenched. The aforementioned annealing temperatures were chosen such that to avoid the formation of any possible second phases such as sigma (s) phase that is popularly formed in equiatomic CoCrFeMnNi (Fe20) when annealed at temperatures below 800 °C [22].

2.3. Microstructural characterization

Characterization of the microstructure was done using scanning electron microscopy on a backscatter mode (SEM-BSE). After annealing, samples for SEM observation were mechanically polished up to #2400 SiC paper and then electro-polished in a solution made of 90% perchloric acid and 10% acetic acid with a voltage of 15 V for 3 min. The grain size from the SEM micrographs was obtained by line intercept method counting annealing twins as a boundary. An average of 5 micrographs was used to calculate the grain size in each condition. A summary of the grain size is shown in Table 1.

2.4. Mechanical testing

To investigate the mechanical properties of Fe20, Fe40, Fe50, and Fe60 alloys, room temperature tensile testing was carried out using dog-bone shaped specimens at a strain rate of 8×10^{-4} s^{-1}. The dimensions of tensile specimens were sectioned from annealed samples parallel to the rolling direction using electrical discharge machining having gauge dimensions of 10 $\times$ 2.5 $\times$ 1 mm^3. The thickness of the tensile specimens was achieved by mechanical thinning using SiC paper to obtain a mirror-like surface. A white spray followed by small amounts of black spray were applied to obtain a speckle pattern for precise strain measurement using digital image correlation technique.

3. Results and discussion

3.1. Microstructure

The microstructure of the representative samples of the Fe20–Fe60 is shown in Fig. 1. The micrographs (a)- (d) show the microstructure of specimens annealed at 900 °C for 3 min while (e) – (h) show that of specimens after long-term annealing of 10 h at 1000 °C. It is interesting the note that even 3 min of annealing is enough to fully recrystallize the alloys under study and induce grain growth at the same time. This indicates faster recrystallization kinetics primarily due to the high temperature involved [23]. The average grain size obtained from the above heat treatment condition was about ~3.6 μm as shown in Table 1. Moreover, it is noteworthy that the mean grain size remains fairly the same regardless of the composition (increment of Fe content) and also that the grain growth kinetics are quite slow even on the non-equiatomic alloys such as Fe40– Fe60. In fact, their calculated grain growth exponent, n, for the four alloys falls in the region of ~2.8 ± 0.35 (not shown here) at 900 °C, which is similar to that of the equiatomic CoCrFeMnNi (~2.8–3.08) reported in other studies [17,24,25]. The small difference between the value in the present study and others studies can be attributed to the difference in alloy preparation and annealing temperatures. However, the effect of this difference can be ignored since it is not significantly high. Therefore, it can be deduced that the change of Fe

Table 1
Grain sizes of Fe20 – Fe60 alloys annealed at 900 °C and 1000 °C for 3 min–10 h The grain size was measured using the line-intercept method on at-least five micrographs for each condition. Annealing twins were counted as a boundary.

Temperature (°C)	Annealing time	Grain size (μm)			
		Fe20	Fe40	Fe50	Fe60
900	3 min	3.3 ± 1.4	3.7 ± 1.7	3.7 ± 1.9	4.4 ± 2.0
	15 min	6.7 ± 2.3	7.8 ± 2.1	8.2 ± 2.6	6.3 ± 3.4
	1 h	11.2 ± 2.5	9.5 ± 2.9	10.1 ± 2.1	12.1 ± 2.2
	2 h	16.7 ± 3.2	16.0 ± 2.8	15.7 ± 3.7	18.6 ± 3.8
1000	2 h	39.4 ± 1.8	41.5 ± 2.4	42.3 ± 3.5	37.5 ± 4.2
	4 h	50.9 ± 3.4	50.9 ± 3.3	49.9 ± 2.3	52.7 ± 2.9
	10 h	56.2 ± 4.4	57.0 ± 2.4	54.0 ± 3.3	56.9 ± 2.8

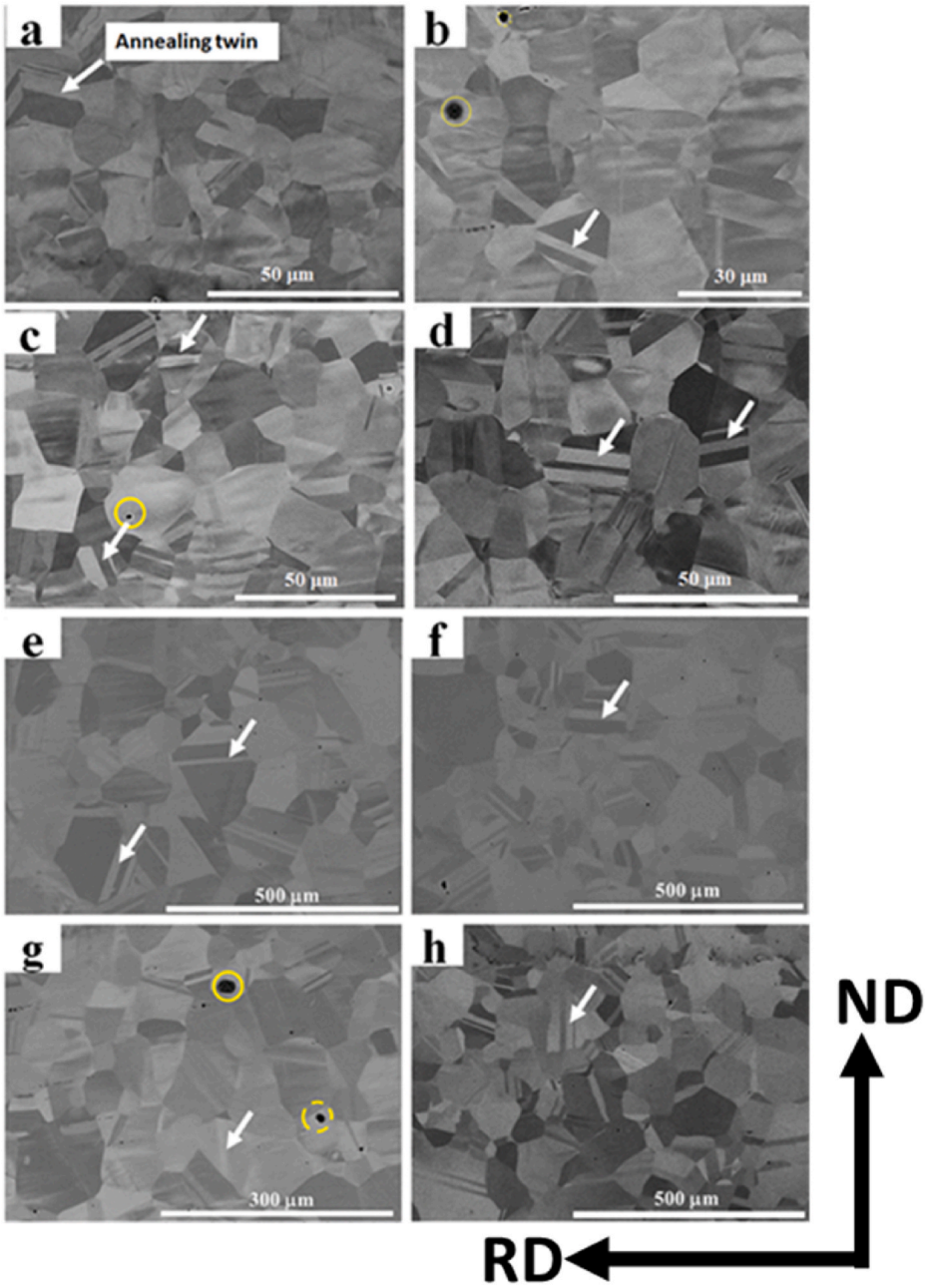

Fig. 1. Representative SEM-BSE images of specimens annealed at 900 °C for 3 min (a–d), and 1000 °C for 10 h (e–h). Fe20 (a, b), Fe40 (c, d), Fe50 (e, f), and Fe60 (g, h). The arrows (white) show the annealing twins while the yellow circles indicate a possible Mn oxides.

content has no significant effect on the grain growth behavior of the studied $CoCrMnNi)_{100-x}$ Fe_x and that the sluggish diffusion effect reported in Fe20 is fairly maintained by the alloys with higher Fe content [17].

Annealing twins, identified by the white arrow, were observed in all the specimens shown in Fig. (a)–(h) and even in those micrographs not shown here. In addition, it was observed that their density tends to be high in Fe60 specimens especially those annealed in short periods as in the case of Fig. 1d. Nearly every grain in Fe60 specimen annealed at 900 °C for 3 min contains an annealing twin unlike in Fe20, Fe40, and Fe50. Jin et al. studied the development of annealing twin during recrystallization and grain growth of pure nickel and concluded that the annealing twin density increases during recrystallization whereas it decreases during grain growth [26,27]. A similar phenomenon can be observed in the present study where specimens with high density of annealing twins correspond to those with short annealing periods after recrystallizations has just been completed. However, after 10 h of annealing, the density of annealing twins tend to be low.

The black spots shown in Fig. 1 (b,c, and g) are oxides mainly from the Mn, which is known to be prone to oxide formation according to Energy-dispersive X-ray spectroscopy analysis (not shown here). It is possible the environment in the arc-melting machine is not entirely a vacuum. A quick analysis of the micrographs presented in Fig. 1, and X-ray diffraction patterns (not shown here) indicate that the alloys are a single-phase fcc at all annealing conditions. This is also confirmed from previous theoretical calculations and experimental reports that heat treatment of CoCrFeMnNi-based HEAs and MEAs resulted in a single phase fcc microstructure [28].

3.2. Mechanical properties

The engineering stress strain curves of Fe20 – Fe60 alloys tensile tested at room temperature are shown in Fig. 2. The YS decreases as the grain size increases according to the classical HP relationship [29]. It should be noted that to obtain a good regression analysis of the HP parameters, specimens with a large scatter were excluded from the graphs. In our previous report [30], the effect of Fe on the SS strengthening of $CoCrMnNi)_{100\text{-}x}Fe_x$ MEAs and HEAs was investigated using theoretical models. In that study, the effect of other strengthening mechanisms (PP, and GB strengthening) was not taken into consideration simply because there was no precipitates observed in the microstructure and the fact that the specimens used for tensile testing had nearly equal grain size, respectively. The yield strength of a material is affected by the following strengthening mechanisms: SS strengthening ($\Delta\sigma_{SS}$), GB strengthening ($\Delta\sigma_{GB}$), and PP hardening ($\Delta\sigma_P$), as shown below.

$$\sigma_y = \Delta\sigma_{SS} + \Delta\sigma_{GB} + \Delta\sigma_P \quad (2)$$

The precipitation hardening term on right hand side of Eq. (2) can be ignored since the alloys exhibited single-phase fcc according to the x-ray diffraction technique (not shown here). Therefore, the main strengthening mechanisms of these MEAs and HEAs are SS and GB strengthening. Unlike the GB strengthening, the effect of solid solution term is well documented in Ref. [30], where it was found that the increment of Fe content 'dilutes' the complex concentrated nature of HEAs. The dilution leads to a less distorted crystal lattice as a result of decreased atomic size misfit parameter, hence, decreased YS. The average grain used for the previous study was approximately 6.35 μm [30]. It is interesting that the YS of Fe20, Fe40, Fe50, and Fe60 HEAs and MEAs with an average grain size of 3.6 μm showed a similar tendency in the present study as shown in Fig. 2e. A simple extrapolation of the point of intersection between YS and total elongation (TE) shows that $Fe_{37}(CoCrMnNi)_{63}$ could potentially be an optimal composition for strength-ductility balance. Moreover, Zhang et al. [31] investigated local structural distortion induced by chemical complexity in CoCrFeMnNi HEA and established that static atomic displacement parameter for this alloy at 0 K to be 0.035–0.041 Å, which is higher than that of pure Ni. In addition, Mn was reported to exhibit large bond distances with neighboring atoms compared to other atoms (Co, Cr, Fe, Ni) using

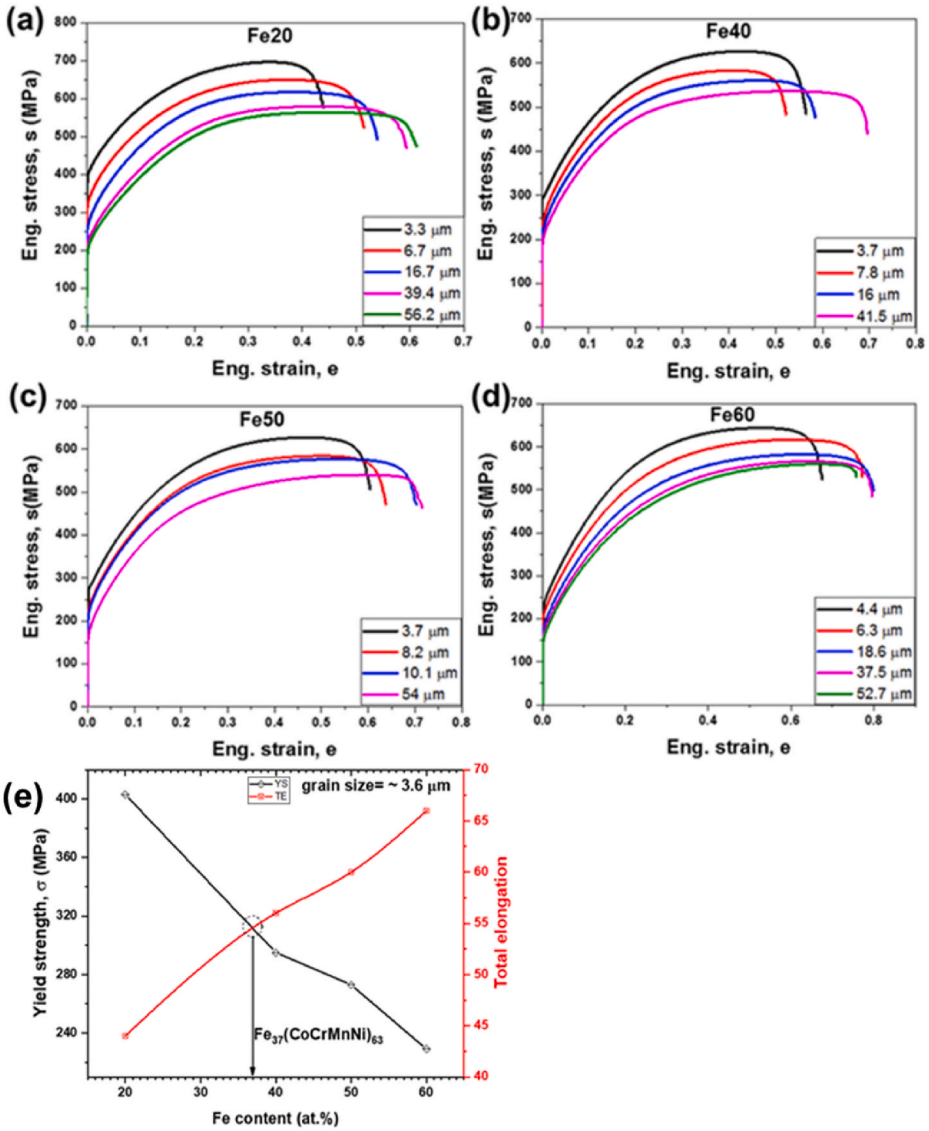

Fig. 2. Tensile properties of $(CoCrMnNi)_{100\text{-}x}$ Fe_x HEAs/MEAs. (a)–(d) Shows the engineering stress-strain curves of (a) Fe20, (b) Fe40, (c) Fe50, and (d) Fe60 obtained at room temperature from various grain sizes. (e) Yield strengths of Fe20, Fe40, Fe50, and Fe60 from specimens with same grain size (~3.6 μm) to show the effect of solid solution strengthening.

extended X-ray absorption fine structure measurements. A similar conclusion was drawn by Yoshida et al. [18]about Mn atoms, who also proposed an elemental – elemental combination as an additional strengthening mechanism in MEAs and HEAs. In their study on quantitative determination of the lattice constant in HEAs using XRD, Wang et al. [32] highlighted that Cr atom plays a superior role in SS strengthening compared to the other principal elements in CoCrFeNi HEA. Therefore, increasing the Fe content in the present study, leads to a proportional decrease of Mn and Cr elements, which are known to play a superior role in SS strengthening.

3.3. Grain boundary strengthening

The classical HP relationship, as denoted by Eq. (1), is widely used to describe GBstrengthening [33,34]. The HP equation can show the effect of both SS and GB strengthening using the first and second terms on the right hand side of Eq. (1).

One of the unique characteristic of HEAs is their indistinguishable matrix and solute compared to conventional alloys, a feature that is mainly attributed to the presence of more principal elements. As a result, the large atomic size misfit due to different atomic sizes of the principal elements involved induces severe lattice distortion to their crystal lattice. Therefore, it becomes difficult to introduced new dislocations in a severely distorted crystal lattice, hence contributing to high YS reported in HEAs, especially, in the equiatomic compositions [35,36]. Therefore, SS strengthening in HEA has a direct relationship with lattice distortion of the alloy. Consequently, SSstrengthening in MEAs and HEAs can be evaluated theoretically using a model initially developed by Toda et al. [37] and later refined by Yoshida et al. [18], which predicts their lattice distortion by evaluating their average atomic size misfit. This model was successfully used on our previous report [30]. Moreover, solid solution in MEAs and HEAscan also be obtained experimentally from the friction stress term of the HP relationship as shown in Eq. (2). The values of friction stress and HP coefficient were obtained by fitting the data points of YS versus the inverse square root of the grain size, as shown in Fig. 3. The values of friction stress for Fe20, Fe40, Fe50, and Fe60 are 194 MPa, 169 MPa, 159 MPa, and 149 MPa, respectively. These values are also plotted as a function of Fe content and compared with other MEAs and HEAs in literature, as shown in Fig. 3e. It is evident that the decrease in friction stress as a function of the Fe content is monotonic and that the highest decrement (25 MPa) is observed after adding 20 at.% of Fe to the equiatomic CoCrFeMnNi HEA. This agrees excellently with the

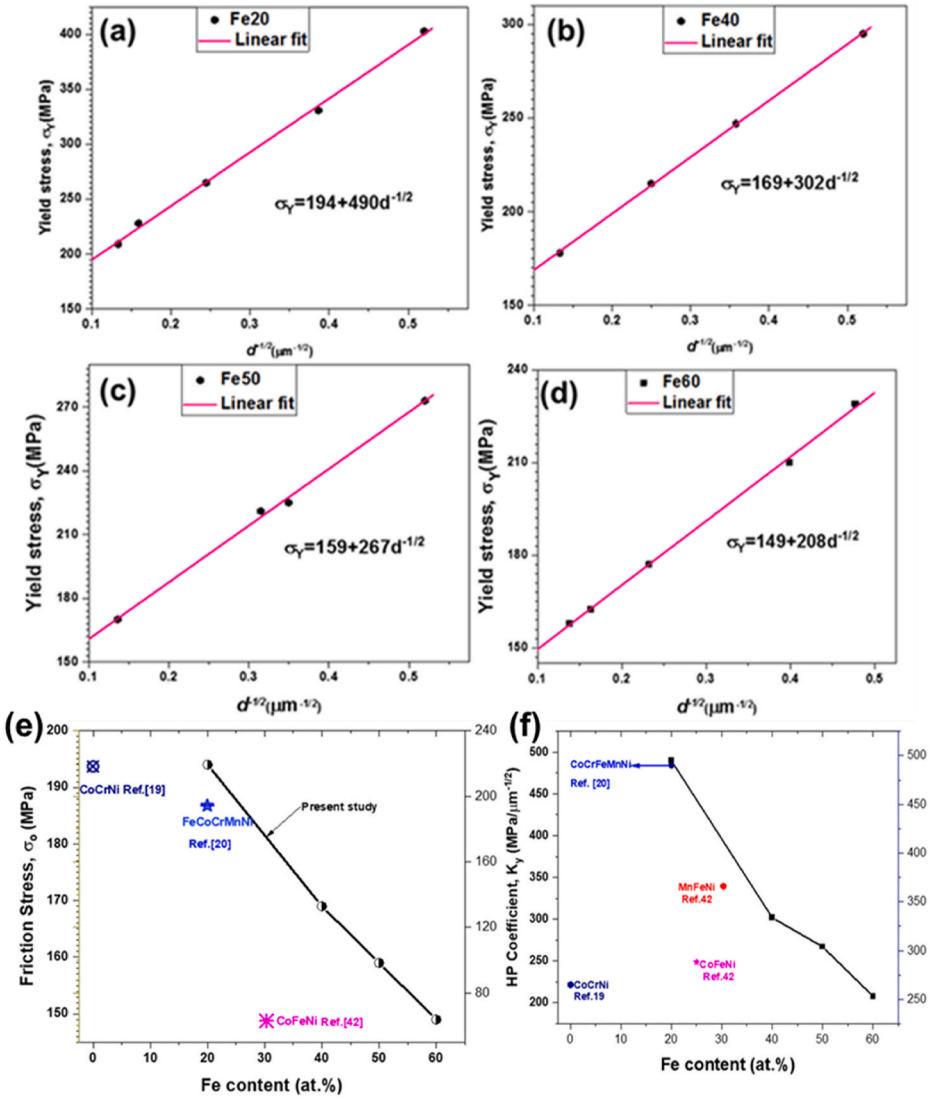

Fig. 3. (a)–(d) Hall-Petch relationship plots of (a) Fe20, (b) Fe40, (c) Fe50, and (d) Fe60, respectively. (e) Shows the friction stress (σ_o), and (f) Hall-Petch coefficient (K_y) as a function of the Fe content as obtained from y-intercept and slope of graphs (a)–(d), respectively. Other values from literature [19-21,40,41,42] have been added to (e) and (f) for comparison.

theoretical calculation which also predicted that the decrease in atomic size misfit, hence lattice distortion, is largest when the composition changes from Fe20 to Fe40 while the change from Fe40 to Fe50 and finally to Fe60 is minimal, which corresponds to approximately 5.9%. Therefore, it can be deduced that at higher Fe content the crystal lattice becomes less distorted, and as a result the contribution of SS strengthening also becomes weak. This phenomenon translates to low YS of non-equiatomic MEAs and HEAs compared to their equiatomic counterparts [38]. Moreover, recently Yoshida et al. [39] proposed short range order or short range clustering (SRO or SRC) as an additional strengthening mechanism in MEAs and HEAs compared to the conventional alloys or dilute alloy systems. This additional hardening was attributed to preferential element-element combination, which increases significantly, the average potential energy for a dislocation in high-alloy systems compared to even dilute alloys having the same or higher average lattice distortions to the high-alloy systems [39].

Interestingly, the slope, which represents the HP coefficient (K_y), decreases as well as the Fe content is increased. The K_y values for Fe20, Fe40, Fe50, and Fe60 are 490, 302, 267, and 208, respectively, as shown in Fig. 3a – d, also showing a monotonic decrease. Therefore, it can be infered that increasing the Fe content weakens both SS strengthening and GB strengthening mechanisms. The HP coefficient is affected by factors such as interstitial atoms (e.g carbon and boron), precipitates, crystallographic texture, temperature and the stacking fault energy (SFE) [21,43,44]. Both interstitial atoms and precipitates tend to segregate to the grain boundaries, therefore, significantly increasing the critical shear stress required for slip transfer from one grain to another [45-47]. However, since the alloys under study have no precipitates nor interstitial elements, their contribution to GB strengthening is excluded. In addition, some researchers have postulated that alloys with low SFE tend to have superior HP coefficient due to reduced cross-slip activity courtesy of enlarged stacking faults in FCC materials [48,49]. Based on this criterion, HEAs with low SFE values should have high HP coefficient values, hence superior GB strengthening. However, sampling a few reports from literature shows that there is no linear relationship between SFE and the HP coefficient. For instance, CoCrFeMnNi and CoCrNi have low SFE values of 26 ± 4.5 mJ/m^{-2} and 18 ± 4 mJ/m^{-2}, respectively, compared to high SFE values reported in Cu–Al and Fe–Ni alloys [50, 51]. Their corresponding values of the HP coefficient are 490 MPa/μm$^{-1/2}$ [20] and 265 MPa/μm$^{-1/2}$ [19]. Furthermore, CoFeNi and MnFeNi with SFE values of 70 mJm^{-2} and 80 ± 20 mJm^{-2} have a corresponding HP coefficients of 288 MPa/μm$^{-1/2}$ [41] and 590 ± 25 MPa/μm$^{-1/2}$ [40], respectively. Based on the SFE criterion, the HP coefficient value of CoCrNi should be slightly higher than that of CoCrFeMnNi HEA while those of CoFeNi and MnFeNi MEAs should be ideally similar because there is no significant difference in their SFE values. Moreover, CoFeNi and MnFeNi should ideally have lower HP coefficients compared to that of CoCrFeMnNi and CoCrNi. Interestingly, MnFeNi MEA has a significantly higher HP coefficient (590 ± 25 MPa/μm$^{-1/2}$) despite having a high SFE (80 ± 20 mJm^{-2}) compared to, for instance, CoCrNi MEA (265 MPa/μm$^{-1/2}$), which has a lower SFE (18 ± 4 mJ/m^{-2}). It is also important to note that the [42] HP coefficient of MnFeNi is even higher than its quinary counterpart, equiatomic CoCrFeMnNi HEA. Therefore, it is evident that in HEA/MEAs, a linear relationship of SFE versus the HP coefficient does not seem to exist. A similar conclusion was deduced in a recent work by Schneider et al. [52], who established that CrFeNi exhibited a high HP coefficient compared to CrMnFeCoNi, CrCoNi, and CrFeCoNi MEA and HEAs, despite having the largest SFE, which is inconsistent with the classical relationship for pure metals and conventional alloys[53] .

The dislocation pile up and grain boundary ledges models have been widely accepted as theoretical models in explaining the origin of dislocations responsible for GB strengthening [54,55]. According to the dislocation pile-up model, dislocations from a Frank-Read source move freely in the grain matrix but their motion and transmission to the neighboring grain is impeded by the presence of GBs. Once the motion of the leading dislocation is prevented by the GBs, the other trailing dislocations form a pile-up, whose length is determined by the grain size. It is important to note that, the stress concentration is highest at the pile-up tip due to forces exerted by individual dislocations behind the leading dislocation. The stress is even higher in coarse-grained microstructure because their pile-up length is longer than in fine grained microstructure. Therefore, only a small value of applied (external) stress will be required to transmit dislocations from the pile-up across the GB or initiate slip in the neighboring grain of a coarse-grained microstructure resulting to a yielding of a polycrystalline material [56]. However, the lack of evidence of dislocation pile-up at the GBs in some polycrystalline materials [57,58], prompted the need for an alternative model to explain the origin of GB and HP relationship. Li [59] proposed GB ledges as the source of dislocations responsible for the GB strengthening. In this model, the GBs emit dislocations, which move to the grain matrix to form forest dislocation. The GB ledges density was found to be inversely proportional the grain size similar to the dislocation pile-up model. Moreover, it was noted that the strength of GB can be interpreted as the stress required to initiate plastic deformation through dislocation generation from the GB ledges to form forest dislocation in the GB vicinity [59]. Interestingly, both experimental and molecular dynamics simulations have revealed that GB ledges are the favorable sources of dislocations [57,60].

Recently Chowdhury et al. [61] used molecular dynamic simulations (MDS) to investigate slip transmission mechanisms in Ni–Co fcc binary alloys across Σ 3 coherent twin boundaries and showed that the transfer of the first dissociated dislocation in a pile up was significantly affected by unstable SFE (γ_{USFE}) than intrinsic SFE (γ_{ISFE}). Borovikov et al. [62] studied the role of stable and unstable SFE on dislocation nucleation and their apparent effect on the YS of nano-crystalline metals. Only a MDS was employed in this study due to the inability to experimentally isolate the effects of SFE without the contribution from other factors like GB sliding and grain rotation. It was postulated that the YS is proportional to both γ_{USFE} and γ_{ISFE}. However, from the present study and the results of Schneider et al. [52], the latter seems to have little effect on the GB strengthening of HEAs and MEAs. In its place, the former (γ_{USFE}) tends to play a decisive role in explaining the unique behaviour and evolution of HP coefficients in HEAs and MEAs. Interestingly, Schneider et al. [52] plotted HP coefficients of HEAs and MEAs derived from CoCrFeMnNi system as a function of γ_{USFE} values calculated by Huang et al. [63], and a linear relationship was observed. Therefore, HEAs and MEAs, with high γ_{USFE} will possess superior HP coefficients and consequently, enhanced GB strengthening. This observation is consistent with the postulations of Borovikov et al. [62]. Based on these findings, it is reasonable to deduce that an increase of Fe content from Fe20 (CoCrFeMnNi) to Fe60, induces a proportional decrease of the γ_{USFE}, which brings about a decrease of the HP coefficient. Furthermore, Tadmor and Bernstein [64], Chowdhury et al. [61]and Borovikov et al. [62] have proposed that the propensity of partial dislocation emission has a strong dependency on the γ_{USFE}, which predisposes the theory of the GB ledges as the source of dislocation, proposed by Li [59] as the ideal theory in explaining the GB strengthening in addition to early evidence by Refs. [57,60].

The present findings of HP coefficient dependence on the γ_{USFE} provides an insight into the role the constituent principal elements and their respective concentrations play on the GB strengthening in HEAs and MEAs. Another notable feature from Fig. 3 e and f, is the decrease of both the SS and GB strengthening as the Fe content is increased, which explains their inferior YS compared to the equiatomic composition. Moreover, an inverse relationship between SS and GB strengthening is observed in other HEAs and MEAs from literature as shown in Fig. 3e and f. Those alloys with high HP Coefficient, hence superior GB strengthening, have a correspondingly weak SS strengthening based on their low friction stress values. Therefore, to design alloys with superior YS an ingenious choice of elements and their respective concentrations are key in optimizing both SS and GB.

4. Conclusion

In the present study, an experimental investigation on the effect of Fe content on SS and GB strengthening of $(CoCrMnNi)_{100-x}$ Fe_x MEAs and HEAs was carried out and the following conclusions can be drawn:

1) Increasing the Fe content while the other four elements remain in equiatomic, SS strengthening is weakened. This is attributed to the reduced lattice friction, which arises from the decreasing atomic size misfit that is responsible for the pronounced lattice distortion hence increasing the difficulty of introducing new dislocations. The proportional decrease of Cr and Mn atoms, which are reported to play a significant role in SS hardening, contributes to the weak lattice distortion.
2) Also, a linear relationship between the Fe content and GB strengthening was established. HEAs and MEAs with high Fe content tend to have a weak GB strengthening as a result of a monotonic decrease of the HP coefficient. Therefore, the low YS values of, say Fe60, can be attributed to both inferior SS and GB strengthening. Based on these findings and some selected results from literature, it is evident that to design alloys with superior YS, ingenious selection of elements and their concentration plays a key role in optimizing SS and GB strengthening.
3) It was established that there is no linear relationship between HP coefficient and intrinsic SFE. The decrease of the HP Coefficient as Fe content is increased was attributed to a proportional increase of unstable SFE.

Data availability

The raw/processed data required to reproduce these findings cannot be shared at this time as the data also forms part of an ongoing study.

CRediT authorship contribution statement

Ibrahim Ondicho: Conceptualization, Methodology, Formal analysis, Investigation, Writing – original draft. **Bernard Alunda:** Data curation, Writing – review & editing. **Nokeun Park:** Supervision, Project administration, Funding acquisition.

Declaration of competing interest

The authors declare that they have no known competing financial interests or personal relationships that could have appeared to influence the work reported in this paper.

Acknowledgement

This study has been supported by the National Research Foundation of Korea funded by the Korean government (Ministry of Science, ICT and Future Planning, MSIP) (NRF-2016M3D1A1023384 (Future Material Discovery Program)).

References

[1] J.-W. Yeh, et al., Nanostructured high-entropy alloys with multiple principal elements: novel alloy design concepts and outcomes, Adv. Eng. Mater. 6 (5) (May 2004) 299–303, https://doi.org/10.1002/adem.200300567.
[2] J.W. Yeh, Recent progress in high-entropy alloys, Ann. Chimie Sci. Matériaux 31 (6) (2006) 633–648, https://doi.org/10.3166/acsm.31.633-648.
[3] C.C. Juan, et al., Solution strengthening of ductile refractory HfMoxNbTaTiZr high-entropy alloys, Mater. Lett. (2016), https://doi.org/10.1016/j.matlet.2016.03.133.
[4] G. Laplanche, P. Gadaud, L. Perrière, I. Guillot, J.P. Couzinié, Temperature dependence of elastic moduli in a refractory HfNbTaTiZr high-entropy alloy, J. Alloys Compd. (2019), https://doi.org/10.1016/j.jallcom.2019.05.322.
[5] E. Ma, X. Wu, "Tailoring heterogeneities in high-entropy alloys to promote strength–ductility synergy, Nat. Commun. (2019), https://doi.org/10.1038/s41467-019-13311-1.
[6] H. Shahmir, M. Nili-Ahmadabadi, A. Shafiee, M. Andrzejczuk, M. Lewandowska, T. G. Langdon, Effect of Ti on phase stability and strengthening mechanisms of a nanocrystalline CoCrFeMnNi high-entropy alloy, Mater. Sci. Eng. (2018), https://doi.org/10.1016/j.msea.2018.04.014.
[7] J.Y. He, et al., A precipitation-hardened high-entropy alloy with outstanding tensile properties, Acta Mater. (2016), https://doi.org/10.1016/j.actamat.2015.08.076.
[8] I. Toda-Caraballo, P.E.J. Rivera-Díaz-del-Castillo, Modelling solid solution hardening in high entropy alloys, Acta Mater. 85 (Feb. 2015) 14–23, https://doi.org/10.1016/j.actamat.2014.11.014.
[9] Z. Li, K.G. Pradeep, Y. Deng, D. Raabe, C.C. Tasan, Metastable high-entropy dual-phase alloys overcome the strength-ductility trade-off, Nature 534 (7606) (2016) 227–230, https://doi.org/10.1038/nature17981.
[10] C.W. Tsai, Y.L. Chen, M.H. Tsai, J.W. Yeh, T.T. Shun, S.K. Chen, Deformation and annealing behaviors of high-entropy alloy Al0.5CoCrCuFeNi, J. Alloys Compd. (2009), https://doi.org/10.1016/j.jallcom.2009.06.182.
[11] W.H. Liu, et al., Ductile CoCrFeNiMo x high entropy alloys strengthened by hard intermetallic phases, Acta Mater. 116 (Sep. 2016) 332–342, https://doi.org/10.1016/j.actamat.2016.06.063.
[12] S. Chen, et al., Grain growth and Hall-Petch relationship in a refractory HfNbTaZrTi high-entropy alloy, J. Alloys Compd. (2019), https://doi.org/10.1016/j.jallcom.2019.04.291.
[13] F. Otto, A. Dlouhý, C. Somsen, H. Bei, G. Eggeler, E.P. George, The influences of temperature and microstructure on the tensile properties of a CoCrFeMnNi high-entropy alloy, Acta Mater. 61 (15) (2013) 5743–5755, https://doi.org/10.1016/j.actamat.2013.06.018.
[14] J. Ding, Q. Yu, M. Asta, R.O. Ritchie, Tunable stacking fault energies by tailoring local chemical order in CrCoNi medium-entropy alloys, in: " Proceedings of the National Academy of Sciences of the United States of America, 2018, https://doi.org/10.1073/pnas.1808660115.
[15] Z. Li, C.C. Tasan, K.G. Pradeep, D. Raabe, A TRIP-assisted dual-phase high-entropy alloy: grain size and phase fraction effects on deformation behavior, Acta Mater. (2017), https://doi.org/10.1016/j.actamat.2017.03.069.
[16] D. Wei, et al., Novel Co-rich high performance twinning-induced plasticity (TWIP) and transformation-induced plasticity (TRIP) high-entropy alloys, Scripta Mater. (2019), https://doi.org/10.1016/j.scriptamat.2019.02.018.
[17] W.H. Liu, Y. Wu, J.Y. He, T.G. Nieh, Z.P. Lu, Grain growth and the Hall-Petch relationship in a high-entropy FeCrNiCoMn alloy, Scripta Mater. 68 (7) (2013) 526–529, https://doi.org/10.1016/j.scriptamat.2012.12.002.
[18] S. Yoshida, T. Ikeuchi, T. Bhattacharjee, Y. Bai, A. Shibata, N. Tsuji, Effect of elemental combination on friction stress and Hall-Petch relationship in face-centered cubic high/medium entropy alloys, Acta Mater. (2019), https://doi.org/10.1016/j.actamat.2019.04.017.
[19] S. Yoshida, T. Bhattacharjee, Y. Bai, N. Tsuji, Friction stress and Hall-Petch relationship in CoCrNi equi-atomic medium entropy alloy processed by severe plastic deformation and subsequent annealing, Scripta Mater. 134 (2017) 33–36, https://doi.org/10.1016/j.scriptamat.2017.02.042.
[20] S.J. Sun, et al., Enhanced strength and ductility of bulk CoCrFeMnNi high entropy alloy having fully recrystallized ultrafine-grained structure, Mater. Des. 133 (Nov. 2017) 122–127, https://doi.org/10.1016/j.matdes.2017.07.054.
[21] Z. Wu, H. Bei, G.M. Pharr, E.P. George, Temperature dependence of the mechanical properties of equiatomic solid solution alloys with face-centered cubic crystal structures, Acta Mater. (2014), https://doi.org/10.1016/j.actamat.2014.08.026.
[22] E.J. Pickering, R. Muñoz-Moreno, H.J. Stone, N.G. Jones, Precipitation in the equiatomic high-entropy alloy CrMnFeCoNi, Scripta Mater. 113 (Mar. 2016) 106–109, https://doi.org/10.1016/j.scriptamat.2015.10.025.
[23] M. Choi, I. Ondicho, N. Park, N. Tsuji, "Strength–ductility balance in an ultrafine-grained non-equiatomic Fe50(CoCrMnNi)50 medium-entropy alloy with a fully recrystallized microstructure, J. Alloys Compd. 780 (Apr. 2019) 959–966, https://doi.org/10.1016/j.jallcom.2018.11.265.
[24] M. Vaidya, A. Anupam, J.V. Bharadwaj, C. Srivastava, B.S. Murty, Grain growth kinetics in CoCrFeNi and CoCrFeMnNi high entropy alloys processed by spark plasma sintering, J. Alloys Compd. (2019), https://doi.org/10.1016/j.jallcom.2019.03.341.
[25] M.V. Klimova, D.G. Shaysultanov, R.S. Chernichenko, V.N. Sanin, S.V. Zherebtsov, N.D. Stepanov, Kinetics of recrystallization and grain growth in an ultra-fine grained CoCrFeNiMn-type high-entropy alloy, J. Phys. Conf. 1270 (1) (2019), https://doi.org/10.1088/1742-6596/1270/1/012053.
[26] Y. Jin, B. Lin, M. Bernacki, G.S. Rohrer, A.D. Rollett, N. Bozzolo, Annealing twin development during recrystallization and grain growth in pure nickel, Mater. Sci. Eng. (2014), https://doi.org/10.1016/j.msea.2014.01.018.
[27] M.A. Meyers, L.E. Murr, A model for the formation of annealing twins in F.C.C. metals and alloys, Acta Metall. 26 (6) (Jun. 1978) 951–962, https://doi.org/10.1016/0001-6160(78)90046-9.
[28] I. Ondicho, et al., "Experimental investigation and phase diagram of CoCrMnNi–Fe system bridging high-entropy alloys and high-alloyed steels, J. Alloys Compd. 785 (May 2019) 320–327, https://doi.org/10.1016/j.jallcom.2019.01.134.
[29] "The Hall-Petch Relationship," *Advanced Materials And Processes*, 2005.
[30] P. Maya, I. Ondicho, D. Jodi, N. Park, U. Lee, Theoretical Evaluation of Solid Solution Interaction in Fex(CoCrMnNi)100-X Medium- and High-Entropy Alloys, " *Materials Science and Engineering A, vol. Unpublishe*, 2019.
[31] F. Zhang, et al., Chemical complexity induced local structural distortion in NiCoFeMnCr high-entropy alloy, Mater. Resear. Lett. 6 (8) (Aug. 2018) 450–455, https://doi.org/10.1080/21663831.2018.1478332.

[32] Z. Wang, et al., Quantitative determination of the lattice constant in high entropy alloys, Scripta Mater. 162 (Mar. 2019) 468–471, https://doi.org/10.1016/j.scriptamat.2018.12.022.
[33] E.O. Hall, The deformation and ageing of mild steel: III Discussion of results, Proc. Phys. Soc. B 64 (9) (1951) 747–753, https://doi.org/10.1088/0370-1301/64/9/303.
[34] N.J. Petch, The cleavage strength of polycrystals, J. Iron Steel Inst. 174 (19) (1953) 25–28, https://doi.org/10.1007/BF01972547.
[35] Q. He, Y. Yang, On lattice distortion in high entropy alloys, Front. Mater. (2018), https://doi.org/10.3389/fmats.2018.00042.
[36] Y. Tong, et al., Local lattice distortion in NiCoCr, FeCoNiCr and FeCoNiCrMn concentrated alloys investigated by synchrotron X-ray diffraction, Mater. Des. (2018), https://doi.org/10.1016/j.matdes.2018.05.056.
[37] I. Toda-Caraballo, A general formulation for solid solution hardening effect in multicomponent alloys, Scripta Mater. 127 (Jan. 2017) 113–117, https://doi.org/10.1016/j.scriptamat.2016.09.009.
[38] H. Oh, et al., Lattice distortions in the FeCoNiCrMn high entropy alloy studied by theory and experiment, Entropy 18 (9) (Sep. 2016) 321, https://doi.org/10.3390/e18090321.
[39] S. Yoshida, T. Bhattacharjee, Y. Bai, N. Tsuji, Effect of elemental combination on friction stress and Hall-petch relationship in medium entropy alloys processed by severe plastic deformation and subseuquent annealing, " *Acta Materialia*, 2019.
[40] M. Schneider, F. Werner, D. Langenkämper, C. Reinhart, G. Laplanche, "Effect of temperature and texture on Hall–Petch strengthening by grain and annealing twin boundaries in the MnFeNi medium-entropy alloy, Metals (2019), https://doi.org/10.3390/met9010084.
[41] X.L. An, et al., Hall-Petch relationship and corrosion behavior of cold-rolled CoNiFe medium entropy alloy, J. Alloys Compd. (2019), https://doi.org/10.1016/j.jallcom.2019.151698.
[42] Z. Wu, Y. Gao, H. Bei, Thermal activation mechanisms and Labusch-type strengthening analysis for a family of high-entropy and equiatomic solid-solution alloys, Acta Mater. 120 (Nov. 2016) 108–119, https://doi.org/10.1016/j.actamat.2016.08.047.
[43] N. Hansen, Hall-petch relation and boundary strengthening, Scripta Mater. (2004), https://doi.org/10.1016/j.scriptamat.2004.06.002.
[44] J. Tang, B. Huang, Y. He, W. Liu, K. Zhou, Factors affecting the Hall-Petch relationship in Ti-Al based alloys, Jinshu Xuebao/Acta Metal. Sin. 38 (2002) 365–368.
[45] Z. Wang, I. Baker, Z. Cai, S. Chen, J.D. Poplawsky, W. Guo, The effect of interstitial carbon on the mechanical properties and dislocation substructure evolution in Fe40.4Ni11.3Mn34.8Al7.5Cr6 high entropy alloys, Acta Mater. (2016), https://doi.org/10.1016/j.actamat.2016.08.072.
[46] J.Y. He, et al., Precipitation behavior and its effects on tensile properties of FeCoNiCr high-entropy alloys, Intermetallics (2016), https://doi.org/10.1016/j.intermet.2016.09.005.
[47] Y. Tong, et al., Outstanding tensile properties of a precipitation-strengthened FeCoNiCrTi0.2 high-entropy alloy at room and cryogenic temperatures, Acta Mater. (2019), https://doi.org/10.1016/j.actamat.2018.11.049.
[48] V. Borovikov, M.I. Mendelev, A.H. King, R. Lesar, Effect of stacking fault energy on mechanism of plastic deformation in nanotwinned FCC metals, Model. Simulat. Mater. Sci. Eng. (2015), https://doi.org/10.1088/0965-0393/23/5/055003.
[49] A.C. Arko, Y.H. Liu, The effect of atomic order on the Hall-Petch behavior in Ni3Fe, Metal. Trans. (1971), https://doi.org/10.1007/BF02913419.
[50] S.F. Liu, et al., Stacking fault energy of face-centered-cubic high entropy alloys, Intermetallics (2018), https://doi.org/10.1016/j.intermet.2017.10.004.
[51] R.E. Schramm, R.P. Reed, Stacking fault energies of fcc fe-Ni alloys by x-ray diffraction line profile analysis, Metal. Trans. A 7 (2) (1976) 359–363, https://doi.org/10.1007/BF02642831.
[52] M. Schneider, G. Laplanche, Effects of temperature on mechanical properties and deformation mechanisms of the equiatomic CrFeNi medium-entropy alloy, Acta Mater. 204 (Feb. 2021) 116470, https://doi.org/10.1016/j.actamat.2020.11.012.
[53] N.L. Okamoto, et al., Size effect, critical resolved shear stress, stacking fault energy, and solid solution strengthening in the CrMnFeCoNi high-entropy alloy, Sci. Rep. 6 (1) (Oct. 2016), https://doi.org/10.1038/srep35863. Art. no. 1.
[54] A.H. Cottrell, B.A. Bilby, Dislocation theory of yielding and strain ageing of iron, Proc. Phys. Soc. 62 (1) (1949) 49–62, https://doi.org/10.1088/0370-1298/62/1/308.
[55] J.D. Eshelby, F.C. Frank, F.R.N. Nabarro, XLI. The equilibrium of linear arrays of dislocations, Lond., Edinburgh, Dublin Philos. Mag. J. Sci. (1951), https://doi.org/10.1080/14786445108561060.
[56] M.F. Ashby, D.R.H. Jones, Strengthening methods and plasticity of polycrystals, Eng. Mater. 1 (2012).
[57] L.E. Murr, Some observations of grain boundary ledges and ledges as dislocation sources in metals and alloys, Metal. Trans. A (1975), https://doi.org/10.1007/BF02658408.
[58] H. Van Swygenhoven, P.M. Derlet, A.G. Frøseth, Stacking fault energies and slip in nanocrystalline metals, Nat. Mater. 3 (6) (Jun. 2004), https://doi.org/10.1038/nmat1136. Art. no. 6.
[59] J.C.M. Li, Petch Relation and Grain Boundary Sources, " *Transactions of the Metallurgical Society of AIME*, 1963.
[60] L. Capolungo, D.E. Spearot, M. Cherkaoui, D.L. McDowell, J. Qu, K.I. Jacob, Dislocation nucleation from bicrystal interfaces and grain boundary ledges: relationship to nanocrystalline deformation, J. Mech. Phys. Solid. 55 (11) (Nov. 2007) 2300–2327, https://doi.org/10.1016/j.jmps.2007.04.001.
[61] P. Chowdhury, H. Sehitoglu, H.J. Maier, R. Rateick, "Strength prediction in NiCo alloys – the role of composition and nanotwins, Int. J. Plast. 79 (Apr. 2016) 237–258, https://doi.org/10.1016/j.ijplas.2015.07.002.
[62] V. Borovikov, M.I. Mendelev, A.H. King, Effects of stable and unstable stacking fault energy on dislocation nucleation in nano-crystalline metals, Model. Simulat. Mater. Sci. Eng. 24 (8) (Nov. 2016), 085017, https://doi.org/10.1088/0965-0393/24/8/085017.
[63] H. Huang, et al., Critical stress for twinning nucleation in CrCoNi-based medium and high entropy alloys, Acta Mater. 149 (May 2018) 388–396, https://doi.org/10.1016/j.actamat.2018.02.037.
[64] E.B. Tadmor, N. Bernstein, A first-principles measure for the twinnability of FCC metals, J. Mech. Phys. Solid. 52 (11) (Nov. 2004) 2507–2519, https://doi.org/10.1016/j.jmps.2004.05.002.